Adaptive Feedback Linearization control of SynRM drives with on-line inductance estimation

Angelo Accetta, *Member IEEE,* Maurizio Cirrincione, *Senior Member IEEE,* Filippo D'Ippolito, *Member IEEE.* Marcello Pucci, *Senior Member IEEE,* and Antonino Sferlazza, *Member IEEE.*

***Abstract*—This paper proposes an adaptive input-output Feedback Linearization Control (*FLC*) techniques for Synchronous Reluctance Motor (*SynRM*) drives, taking into consideration the iron losses. As a main original content, this work proposes a control law based on a new dynamic model of the *SynRM* including iron losses as well as the on-line estimation of the static inductances. The on-line estimation of the *SynRM* static inductances permits to inherently take into consideration the magnetic saturation phenomena occuring on both axes. As a major result, it permits a null stator current steady state tracking error even with a proportional derivative controller. The estimation law is obtained thanks to a Lyapunov-based analysis and thus the stability of the entire control system, including the estimation algorithm, is intrinsically guaranteed. The proposed adaptive *FLC* technique, has been tested experimentally on a suitably developed test set-up, and compared experimentally with its non-adaptive versions in both tuned and detuned working conditions. Moreover, a sensitivity analysis of the performance of the adaptive *FLC* to the variations of the stator resistance at low speed has been made. Finally, an analysis of the effects of the iron losses on the control performance and stability at high speed in the field weakening region at medium/high loads has been made.**

***Index Terms*—Synchronous reluctance motor *SynRM*, feedback linearization control *FLC*, inductances estimation, adaptive system.**

I. Introduction

The first prototypes of the synchronous reluctance motors (*SynRM*) date back to the first decades of 1900. Initially, *SynRMs* have been rarely adopted because of their relatively low performance, in terms of output torque and power densities, combined with their high price. Only recently, more performing *SynRMs* have been designed and manufactured at an industrial level, presenting a much more reliable and robust construction. With increased values of the saliency ratios (9-12) [2]. As a matter of fact, *SynRMs* manufactured with high saliency ratios are particularly suited for high performance applications, like machine tools drives, robotics, and electrical vehicles. Because of their constructional characteristics, *SynRMs* can be hardly operated in open loop. Nevertheless, high-dynamic performance can be achieved by adopting vector control technique, and several rotor-oriented or stator flux-oriented control schemes have been developed [3]–[5]. The theoretical performance of the *SynRMs* is limited, however, by the strong magnetic non-linearity of the machine, with different self-saturation phenomena on the direct and quadrature axes, as well as significant cross-saturation phenomena. To cope these issues, the control system theory offers an important corpus of nonlinear control methodologies for dealing with nonlinear systems. Despite this, very few applications of nonlinear control methods for electrical drives are, in general, present in scientific literature, and even less to *SynRMs*.

With regards to high-performance synchronous reluctance motor (*SynRM*) drive, some examples are illustrated below. In particular, [6] proposes a novel adaptive complementary sliding mode speed control and an effective d-axis current control in order to increase performances by dealing with highly nonlinear and time-varying *SynRM* dynamics at the varied load torque conditions. In [7] the design and implementation of a current controller for a *SynRM* is described based on continuous control set nonlinear model predictive control. Here, instead of using an explicit magnetic model, a computationally efficient gray box model of the flux linkage map is proposed and employed. Differently from this work, in [8] a direct discrete-time variant of the flux-linkage-based current controller is developed by exploiting, the nonlinear magnetic saturation characteristics of a *SynRM*. This makes the controller more complex and with a higher computational burden, but it allows a more accurate flux tracking. An interesting comparison among the most common high performance control strategies of *SynRMs* is presented in [9], where field-oriented control, direct torque control, and finite-set model-predictive control are compared by simulations.

However, among the various non-linear control techniques, one of the most promising is the so-called input-output Feedback Linearization Control (*FLC*) [10]–[14]. In particular, [11], [12] propose an adaptive input-output feedback-linearization (*AIOFL*) technique used for speed and torque-tracking control of a *SynRM* drive. [13] proposes a nonlinear controller, able to directly regulate the torque by selecting the product of direct and quadrature axes currents as one of

Manuscript received mm dd, yyyy; revised mm dd, yyyy; accepted mm dd, yyyy.

This work was supported by in part by ARS01_00333 TETI, CUP under Grant 45F21000050005 and in part by PON02_00153_2939517 TESEO, CUP under Grant B61C12000850005.

This paper has been previously presented and published, in a preliminary version, in a Conference Proceedings sponsored by the IEEE Industry Application Society: IEEE Energy Conversion Congress and Exposition 2020 (ECCE 2020) [1].

A. Accetta and M. Pucci are with the INstitute for Marine engineering (INM), section of Palermo, National Research Council of Italy (CNR), Via Ugo La Malfa 153, 90146 Palermo, Italy (e-mail: angelo.accetta@cnr.it, marcello.pucci@cnr.it).

M. Cirrincione is with the School of Engineering and Physics, University of the South Pacific, Laucala Campus, 0679 Suva, Fiji (e-mail: cirrincione_m@usp.ac.fj).

F. D'Ippolito and A. Sferlazza are with the Department of Engineering, University of Palermo, Viale delle Scienze, 90128 Palermo, Italy (e-mail: filippo.dippolito@unipa.it, antonino.sferlazza@unipa.it).

the output variables. Recently, a nonlinear controller based on input-output *FLC* for *SynRMs* drives has been proposed, which takes into consideration the self and cross-saturation saturation effects [15]. The space-vector dynamic model adopted for developing the proposed *FLC* technique has been proposed in [16], and the related magnetic model including both the self and cross-saturation in [17]. The *FLC* is, however, a model-based control, and thus, suffers primarily from two disadvantages: 1) the accuracy of the dynamic model on which the control law is based; and 2) the corresponding correct knowledge of the model parameters.

Starting from these considerations, this paper proposes an adaptive input-output feedback linearization technique for SynRMs, taking into consideration the magnetic saturation by the on-line estimation of the direct and quadrature static inductances. The on-line estimation of the direct and quadrature inductances is integrated in the control action and permits the magnetic saturation to be inherently considered. As a major result, it permits a null current steady state tracking error even with a proportional derivative controller. The estimation law is derived from a Lyapunov based approach so as to intrinsically guarantee the stability of the entire control system, including the estimation algorithm. Furthermore, the dynamic model underlying the proposed non-linear adaptive controller accounts also for the iron losses, that is a further original contribution of the work. It should be noted that few examples of adaptive input-output *FLC* have been proposed in literature [12], [14]; however, differently from those, the model used in this work takes into consideration both self and cross-saturation saturation effects and iron losses.

Moreover, differently from [15], a different controller structure has been adopter in this work. Indeed, in [15] the system was linearized by considering the speed as output, this allows the linearization of the whole electro-mechanical system, but there was not the direct control of the stator current, which was considered as internal variables. In this work, in order to estimate the static inductances, the stator currents are considered as output of the system. This leads to a different strategy because only the electrical part of the system can be linearized and the speed is managed by means of a further external loop. However, the currents are now directly controllable as will be shown in the paper. Moreover, this paper gives an explicit tuning rule to determine the controller parameters in order to ensure a well-defined convergence speed of the current tracking errors as well as the inductance estimation errors. With such an approach even the on-line variation of the inductances with the current (due to saturation effects) can be accounted for. The proposed control technique has been tested experimentally on a suitably developed test set-up, and compared experimentally with its non-adaptive version.

The manuscript is organized as follows. Section II describes the adopted dynamic model of the *SynRM* considering the magnetic saturation (both self and cross-saturation) and the iron losses. Section III describes the proposed adaptive FLC technique. Section IV describes the adopted test set-up and finally section V describes the experimental results.

This paper is an improvement and evolution of [1].

II. Space-vector model of the *SynRM* considering self and cross-saturation and iron losses

A. Proposed magnetic model

The proposed magnetic model is in the framework of a flux versus current approach, so it is suitable for dynamic models of *SynRMs* adopting the stator currents as state variables. As for the magnetic characteristics of the *SynRM*, the following functions are proposed, which consider both the self and cross-saturation effects and describe the relationships between the direct and quadrature components of the stator fluxes and the corresponding components of the stator currents in the synchronous reference frame. The stator flux direct (x) and quadrature (y) components have been defined as follows:

$$\psi_{sx} = 2\alpha_1\left(\frac{1}{1+\mathrm{e}^{-\beta_1 i_{mx}}}-\frac{1}{2}\right)+\eta_1 i_{mx}+\Delta\psi_{sx} \tag{1a}$$

$$\psi_{sy} = 2\alpha_2\left(\frac{1}{1+\mathrm{e}^{-\beta_2 i_{my}}}-\frac{1}{2}\right)+\eta_2 i_{my}+\Delta\psi_{sy} \tag{1b}$$

In particular, as for the self-saturation, it has been formulated adopting sigmoid functions, to which linear functions are added because the magnetic characteristic of the motor is not completely flat in deep saturation. As for the cross-saturation, it has been conceived starting from the definition of a proper co-energy variation function due to the cross-saturation. The co-energy variation function has been expressed as the product of two functions, one depending only on i_{mx} and the other depending only on i_{my}. This last condition is very important since it permits the reciprocity conditions to be properly fulfilled. The mathematical formulation has been created based on the analysis of [18, Fig. 2]. This last figure shows that the flux on the x axis reduces for increasing values of the current i_{my}. Moreover, for a given value of i_{mx}, the amount of reduction of the flux on the x axis depends on the absolute value of i_{my}, being independent from its sign. The higher the absolute value of i_{my} is, the higher the flux reduction on the x axis is. Moreover, the same figure shows that the flux variation on the x axis is null for zero value of i_{mx}, very little for high values of i_{mx}, while it presents a maximum for a certain intermediate range of i_{mx}. These considerations suggest to define the co-energy variation functions as follows:

$$\Delta W' = \gamma\frac{1}{\left(1+\mathrm{e}^{\frac{-s_{mx}}{\sigma_1}}\right)}\frac{1}{\left(1+\mathrm{e}^{\frac{-s_{my}}{\sigma_2}}\right)}. \tag{2}$$

where:

$$s_{mx} = (i_{mx}-\mu_1\mathrm{sgn}(i_{mx}))\mathrm{sgn}(i_{mx}),$$
$$s_{my} = (i_{my}-\mu_2\mathrm{sgn}(i_{my}))\mathrm{sgn}(i_{my}),$$

From (2) the cross-saturation flux variation terms can be computed as:

$$\Delta\psi_{sx} = \frac{d\Delta W'}{di_{mx}} = -\frac{\gamma}{\sigma_1}\frac{\mathrm{sgn}(i_{mx})}{\left(\mathrm{e}^{\frac{s_{mx}}{2\sigma_1}}+\mathrm{e}^{-\frac{s_{mx}}{2\sigma_1}}\right)^2}\frac{1}{1+\mathrm{e}^{-\frac{s_{my}}{\sigma_2}}}, \tag{3a}$$

$$\Delta\psi_{sy} = \frac{d\Delta W'}{di_{my}} = -\frac{\gamma}{\sigma_2}\frac{\mathrm{sgn}(i_{my})}{\left(\mathrm{e}^{\frac{s_{my}}{2\sigma_2}}+\mathrm{e}^{-\frac{s_{my}}{2\sigma_2}}\right)^2}\frac{1}{1+\mathrm{e}^{-\frac{s_{mx}}{\sigma_1}}}. \tag{3b}$$

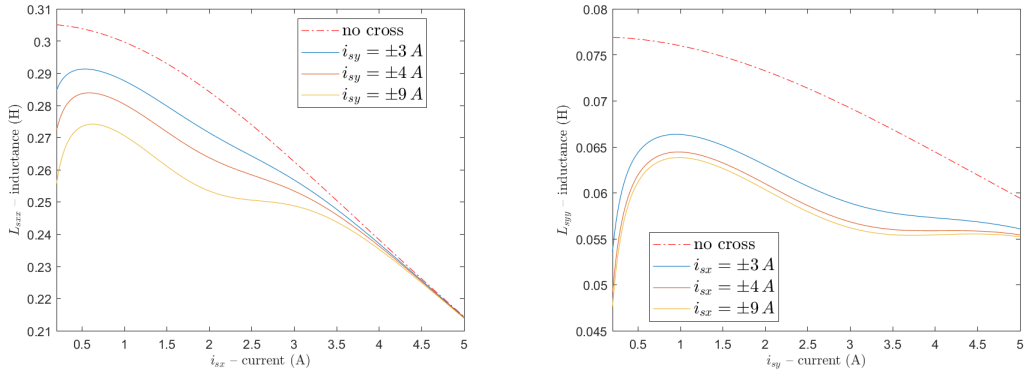

Fig. 1. Static self-inductance on the direct axis, L_{sx}, and on the quadrature axis, L_{sy}, for several values of the current.

Since the nonlinear inductor should not generate or dissipate electrical energy, the reciprocity condition must be satisfied [19], [20]. Starting from these considerations the static inductance components can be defined as follows:

$$L_{sx} = \eta_1 + 2\alpha_1 \left(\frac{1}{1+\mathrm{e}^{-\beta_1 i_{mx}}} - \frac{1}{2} \right) \frac{1}{i_{mx}} - \left(\frac{\gamma}{\sigma_1} \frac{1}{i_{mx}} \frac{\mathrm{sgn}(i_{mx})}{\left(\mathrm{e}^{\frac{s_{mx}}{2\sigma_1}} + \mathrm{e}^{-\frac{s_{mx}}{2\sigma_1}} \right)^2} \right) \left(\frac{1}{1+\mathrm{e}^{-\frac{s_{my}}{\sigma_2}}} \right), \quad (4)$$

$$L_{sy} = \eta_2 + 2\alpha_2 \left(\frac{1}{1+\mathrm{e}^{-\beta_2 i_{my}}} - \frac{1}{2} \right) \frac{1}{i_{my}} - \left(\frac{\gamma}{\sigma_2} \frac{1}{i_{my}} \frac{\mathrm{sgn}(i_{my})}{\left(\mathrm{e}^{\frac{s_{my}}{2\sigma_2}} + \mathrm{e}^{-\frac{s_{my}}{2\sigma_2}} \right)^2} \right) \left(\frac{1}{1+\mathrm{e}^{-\frac{s_{mx}}{\sigma_1}}} \right). \quad (5)$$

where α_1, β_1, η_1, γ, μ_1, σ_1, α_2, β_2, η_2, μ_2 and σ_2 are considered the parameters of the magnetic behavior of the machine. For further details related to the dynamic model of the *SynRM* including both magnetic saturation and iron losses, the reader che refer to [21].

Note that the proposed functions properly satisfy the reciprocity conditions as for the cross-saturation, ensuring that the nonlinear inductances do not generate or dissipate energy. Fig. 1 shows the static inductance curves $L_{sx} = f_1(i_{sx})$ parametrized on i_{sy} and $L_{sy} = f_1(i_{sy})$ parametrized on i_{sx} for the *SynRM* drive under test, whose rated data are shown in Tab. I and whose magnetic model parameters are shown in Tab. II. All the model parameters have been identified by stand-still tests and based on Genetic Algorithms (*GA*) [21].

B. Dynamic model of the SynRM

If $\mathbf{\Psi}_s = [\psi_{sx}, \psi_{sy}]$ is the stator flux space-vector whose direct and quadrature components are expressed in the rotor reference frame with axis on the minumum reluctance path, $\mathbf{i}_s = [i_{sx}, i_{sy}]$ is the corresponding stator current vector and $\mathbf{u}_s = [u_{sx}, u_{sy}]$ is the stator voltage vector, the space-vector dynamic model of the *SynRM* in state form, accounting also for the iron losses, selecting the stator fluxes as state variables, can be written as [21]:

$$\frac{d\mathbf{\Psi}_s}{dt} = -\left(\frac{R_s R_0}{R_s + R_0} \mathbf{L}_s^{-1} + jp\omega_r \right) \mathbf{\Psi}_s + \frac{R_0}{R_s + R_0} \mathbf{u}_s. \quad (6)$$

where R_s and R_0 are respectively the stator and iron losses resistances, p is the pole pairs number, ω_r is the rotor speed and $\mathbf{L}_s = \begin{bmatrix} L_{sx} & 0 \\ 0 & L_{sy} \end{bmatrix}$ is the static inductance matrix. It should be minded that the stator current components, because of the presence of the iron losses, cannot be straightforwardly derived from the corresponding flux components typically computed as $i_{sx} = L_{sx}^{-1}\psi_{sx}$ and $i_{sy} = L_{sy}^{-1}\psi_{sy}$. They must be obtained on the basis of the following relationship involving the stator voltage:

$$\mathbf{i}_s = \frac{R_0}{R_s + R_0} \mathbf{i}_m + \frac{1}{R_s + R_0} \mathbf{u}_s = = \frac{R_0}{R_s + R_0} \mathbf{L}_s^{-1} \mathbf{\Psi}_s + \frac{1}{R_s + R_0} \mathbf{u}_s, \quad (7)$$

where $\mathbf{i}_m$ is the magnetizing current space-vector, and depends on the direct and quadrature components of the magnetizing current i_{mx}, i_{my} that, in this case, differ from the stator current components. In particular, $\mathbf{i}_s = \mathbf{i}_m + \mathbf{i}_0$, where $\mathbf{i}_0$ is the part of the stator current responsible for the iron losses.

Finally the mechanical equation of the *SynRM* is given by:

$$J\frac{d\omega_r}{dt} = -f_v\omega_r + t_m - t_l, \quad (8)$$

where J and f_v are the inertia moment and the viscous friction coefficient, t_l is the load torque, and t_m is the electromagnetic torque generated by the motor and given by:

$$t_m = \frac{3}{2} p \left(\mathbf{\Psi}_s \wedge \mathbf{i}_m \right) = \frac{3}{2} p \left(L_{sx} - L_{sy} \right) i_{mx} i_{my}. \quad (9)$$

It is interesting to note that only the expression of the static inductances appears in the dynamics of the speed, and it depends on the dynamic inductances only indirectly by means of the stator fluxes. As for the impact of the dynamic inductances on the dynamics of the system, the reader can refer to [16].

As shown above, the model of the machine is highly nonlinear and complex, requiring the knowledge of many parameters and the related identification. For this reason a model based control technique, such as *FLC*, requires an accurate identification technique. To make the control algorithm more

robust with respect to the parameter variation and/or accuracy in the identification procedure, an adaptive input-output *FLC* is proposed, where the static inductances L_{sx} and L_{sy} are online estimated, so that the a priori knowledge of the parameters of the magnetic model of the machine is not necessary and, in any case, is robust versus the variation of the inductance themselves (due to saturation or any other phenomena).

III. Adaptive input-output feedback linearization

In order to develop the control algorithm, the equations (6) and (8) can be written in the following form:

$$\frac{d\mathbf{x}}{dt} = \mathbf{f}(\mathbf{x}) + \mathbf{g}(\mathbf{x})\mathbf{u}, \tag{10}$$

$$\mathbf{y} = \mathbf{h}(\mathbf{x}), \tag{11}$$

where $\mathbf{x} = [\psi_{sx},\ \psi_{sy},\ \omega_r]$, $\mathbf{u} = [u_{sx},\ u_{sy}]$, $\mathbf{y} = [\psi_{sx},\ \psi_{sy}]$ and vector fields $\mathbf{f}$, $\mathbf{g}$ and $\mathbf{h}$ are:

$$\mathbf{f}(\mathbf{x}) = \begin{bmatrix} -\frac{R_s R_0}{R_s+R_0} i_{sx} - p\omega_r L_{sy} i_{sy} \\ -\frac{R_s R_0}{R_s+R_0} i_{sy} + p\omega_r L_{sx} i_{sx} \\ -\frac{f_v}{J}\omega_r + \frac{3p}{2J}\left(\frac{1}{L_{sy}} - \frac{1}{L_{sx}}\right)\psi_{sx}\psi_{sy} \end{bmatrix},$$

$$\mathbf{g}(\mathbf{x}) = \begin{bmatrix} \frac{R_0}{R_s+R_0} \\ \frac{R_0}{R_s+R_0} \\ -\frac{1}{J} t_l \end{bmatrix}, \quad \mathbf{h}(\mathbf{x}) = \begin{bmatrix} \psi_{sx} \\ \psi_{sy} \end{bmatrix}. \tag{12}$$

The computation of the Lie's derivatives, to obtain the state feedback linearization, yields:

$$\mathbf{y} = \mathbf{h}(\mathbf{x}), \tag{13}$$

$$\dot{\mathbf{y}} = \mathcal{L}_f \mathbf{h}(\mathbf{x}) + \mathcal{L}_g \mathbf{h}(\mathbf{x})\mathbf{u} = \begin{bmatrix} -\frac{R_s R_0}{R_s+R_0} i_{sx} - p\omega_r L_{sy} i_{sy} \\ -\frac{R_s R_0}{R_s+R_0} i_{sy} + p\omega_r L_{sx} i_{sx} \end{bmatrix} + \begin{bmatrix} \frac{R_0}{R_s+R_0} & 0 \\ 0 & \frac{R_0}{R_s+R_0} \end{bmatrix} \begin{bmatrix} u_{sx} \\ u_{sy} \end{bmatrix}. \tag{14}$$

Note that the relative degree of the system is one. This means that, with this choice of the output, only the stator flux dynamics can be linearized, while the speed dynamics will be considered as zero dynamics, and it can be stabilized by means of a further control action as it will be shown in the following.

Denoting with $\hat{L}_{sx}$ the estimate of L_{sx} and with $\hat{L}_{sy}$ the estimate of L_{sy}, the inductance errors can be defined as follows:

$$\tilde{L}_{sx} = L_{sx} - \hat{L}_{sx}, \qquad \tilde{L}_{sy} = L_{sy} - \hat{L}_{sy}. \tag{15}$$

Using the feedback linearization theory, the state feedback law for system (13) can be obtained as follows:

$$\begin{bmatrix} u_{sx} \\ u_{sy} \end{bmatrix} = \left(\mathcal{L}_g \mathbf{h}(\mathbf{x})\right)^{-1} \left(-\mathcal{L}_f \mathbf{h}(\mathbf{x}) + \begin{bmatrix} u'_x \\ u'_y \end{bmatrix} \right) \tag{16}$$

where u'_x and u'_y are two auxiliary control input that have to be suitably chosen. If the estimated value of inductances is used instead of the real ones, the following two subsystems are obtained from (16):

$$\dot{\psi}_{sx} = p\omega_r i_{sy}\tilde{L}_{sy} + u'_x, \quad \dot{\psi}_{sy} = -p\omega_r i_{sx}\tilde{L}_{sx} + u'_y. \tag{17}$$

One result of this work is to design the control inputs u'_x and u'_y and adaptation laws for inductances $\hat{L}_{sx}$ and $\hat{L}_{sy}$ such that the stator flux components ψ_{sx} and ψ_{sy} track their references and the estimated inductances $\hat{L}_{sx}$ and $\hat{L}_{sy}$ converge to the real ones. In other words, it is necessary to prove the stability of the error in the extended space corresponding to the error variables:

$$\mathbf{e} = \begin{bmatrix} \tilde{\psi}_{sx} \\ \tilde{\psi}_{sy} \\ \tilde{L}_{sx} \\ \tilde{L}_{sy} \end{bmatrix} := \begin{bmatrix} \psi^*_{sx} - \psi_{sx} \\ \psi^*_{sy} - \psi_{sy} \\ L_{sx} - \hat{L}_{sx} \\ L_{sy} - \hat{L}_{sy} \end{bmatrix}, \tag{18}$$

where ψ^*_{sx} and ψ^*_{sy} are the references of the stator fluxes components.

Theorem 1: If the inductance estimation dynamics are selected as:

$$\dot{\hat{L}}_{sx} = -p\omega_r i_{sx}\tilde{\psi}_{sy}, \quad \dot{\hat{L}}_{sy} = p\omega_r i_{sy}\tilde{\psi}_{sx}, \tag{19}$$

and the auxiliary control inputs u'_x and u'_y selected as:

$$u'_x = \dot{\psi}^*_{sx} + k_x\tilde{\psi}_{sx}, \quad u'_y = \dot{\psi}^*_{sy} + k_y\tilde{\psi}_{sy}, \tag{20}$$

for some positive constants k_x and k_y, then the error dynamics $\mathbf{e}$ in (18) converges exponentially to zero, along dynamics (17).

It should be noted that the controller structure defined by eq.s (20) is of the proportioal (P) derivative (D). In particular, there is no integral (I) action. It implies that such a controller structure does not inherently ensure null steady state current error, in particular if the static inductances are not properly known in each working condition. As a matter of fact, a the presence of the on-line inductances estimator inherently ensures a null current steady state tracking error. To obtain a non-null steady state current tracking error with any non-adaptive *FLC*, an exact knowledge of the machine parameters is required. Or, alternatively, a PI controller should be used also for the inner loop. However, this last option would reduce the stability margins and possibly would made the system unstable because the PI introduces a further pole in the origin to the linearized system, which already contains another pole in the origin.

Proof 1: Let's define the following Lyapunov function:

$$V(t) = \frac{1}{2}\mathbf{e}^\top(t)\mathbf{e}(t). \tag{21}$$

By computing the derivative of the Lyapunov function it is obtained:

$$\dot{V}(t) = \mathbf{e}^\top(t)\dot{\mathbf{e}}(t) = \tilde{\psi}_{sx}\dot{\tilde{\psi}}_{sx} + \tilde{\psi}_{sy}\dot{\tilde{\psi}}_{sy} + \tilde{L}_{sx}\dot{\tilde{L}}_{sx} + \tilde{L}_{sy}\dot{\tilde{L}}_{sy}. \tag{22}$$

Replacing expressions (17) in (22), and considering the approximations $\dot{\tilde{L}}_{sx} \approx -\dot{\hat{L}}_{sx}$ and $\dot{\tilde{L}}_{sy} \approx -\dot{\hat{L}}_{sy}$, it results:

$$\dot{V}(t) = \tilde{\psi}_{sx}\left(\dot{\psi}^*_{sx} - p\omega_r i_{sy}\tilde{L}_{sy} - u'_x\right) + \tilde{\psi}_{sy}\left(\dot{\psi}^*_{sy} + p\omega_r i_{sx}\tilde{L}_{sx} - u'_y\right) - \tilde{L}_{sx}\dot{\hat{L}}_{sx} - \tilde{L}_{sy}\dot{\hat{L}}_{sy}. \tag{23}$$

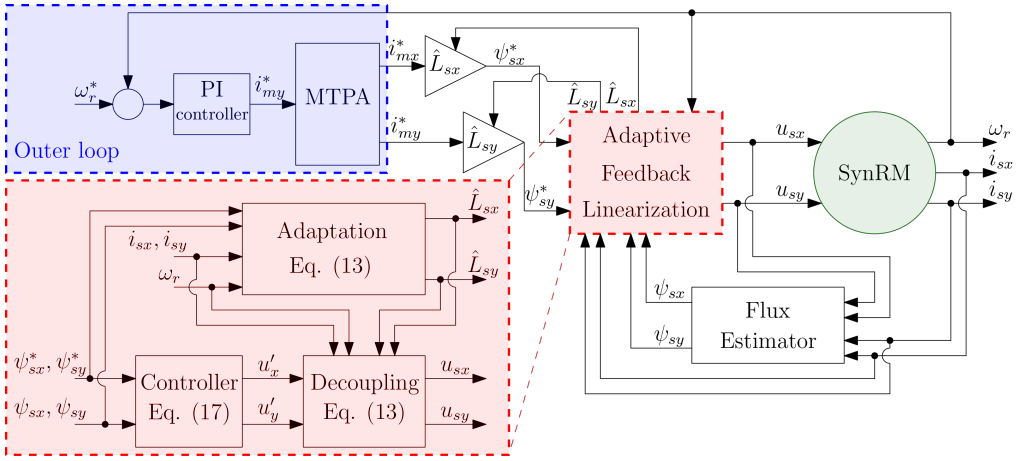

Fig. 2. Block diagram of the proposed control algorithm.

If the auxiliary control inputs u'_x and u'_y are selected as in (20), $\dot{V}(t)$ can be written as follow:

$$\dot{V}(t) = -k_x\tilde{\psi}_{sx}^2 - k_y\tilde{\psi}_{sy}^2 + \tilde{L}_{sx}\left(p\omega_r i_{sx}\tilde{\psi}_{sy} - \dot{\hat{L}}_{sx}\right) + \tilde{L}_{sy}\left(-p\omega_r i_{sy}\tilde{\psi}_{sx} - \dot{\hat{L}}_{sy}\right). \quad (24)$$

If the inductance estimation dynamics are selected as in (19), the last two terms of $\dot{V}(t)$ are zero and consequently:

$$\dot{V}(t) = -k_x\tilde{\psi}_{sx}^2 - k_y\tilde{\psi}_{sy}^2 \leq -k\left(\tilde{\psi}_{sx}^2 + \tilde{\psi}_{sy}^2\right), \quad (25)$$

where $k = \min\{k_x,\ k_y\}$. Since $\dot{V}(t) < 0$, the statement follows. This concludes the proof. □

Remark 1: Note that k in Eq. (25) affects the rate of convergence for the tracking error $\mathbf{e}$. This is an appealing result from practical point of view for the controller designer, because it gives a tuning rule to determine parameters k_x and k_y. Indeed, greater the value of k is, smaller $\dot{V}(t)$ is and consequently faster the convergence speed of the flux tracking errors and of the inductance estimation errors is.

It is noteworthy that the inductance error dynamics on the direct sxis is governed by the flux error on the quadrature axis , and vice versa. It should be further noted that the inductance estimation process is activated only whenever a flux tracking error occurs, in particular in correspondence of speed or torque sudden commands, as it will be shown properly in the experimental tests.

Since the goal is the speed regulation, a further external speed loop is considered. This loop will ensure the stability of the speed, which was considered as zero dynamics in the linearization procedure. Moreover, the Maximum Torque Per Amper (*MTPA*) scheme, proposed in [22], has been integrated in the control scheme in order to obtain both reference values of the currents i_{sx} and i_{sy}. The block diagram of the control systems is shown in Fig. 2. As for the flux estimator block in Fig. 2, the open loop stator flux integration has been performed described by the following equation: $\frac{d\mathbf{\Psi}_s}{dt} = \mathbf{u}_s - R_s\mathbf{i}_s$. The DC drift problems related to the open loop integration of the flux have been solved here adopting the so called neural adaptive integrator proposed in [23].

A. Design of the PI controller of the outer loop

The PI controller of the outer speed loop, shown in Fig. 2, is designed to assign a suitable closed loop dynamics to the system. In particular, it introduces a pole in $s = 0$, which ensures zero steady-state speed error even in the presence of parameter uncertainties, a zero in $s = \frac{k_i}{k_p}$, which allows to assign a suitable phase margin (strictly related with the overshoot) and a gain which allows to fix a well-defined crossover frequency (strictly related with the rise time).

To design the PI controller, it is assumed that the inner loop works correctly and that it is faster than the outer loop. Under these hypotheses, it is possible to consider the following transfer function that describes the plant to be controlled:

$$G_p(j\omega) = \frac{\frac{3}{2}p\left(\frac{1}{L_{sy}} - \frac{1}{L_{sx}}\right)}{j\omega J + f_v}. \quad (26)$$

If the crossover pulsation $\bar{\omega}_t$ and the phase margin $\bar{m}_\phi$ are imposed as specifications, the design of the controller can be carried out by imposing the following conditions:

$$|G_c(j\bar{\omega}_t)||G_p(j\bar{\omega}_t)| = 1, \quad (27a)$$

$$\arg(G_c(j\bar{\omega}_t)) + \arg(G_p(j\bar{\omega}_t)) + \pi = \bar{m}_\phi, \quad (27b)$$

where $G_p(j\omega)$ is given in (26) and $G_c(j\omega)$ is given by:

$$G_c(j\omega) = k_p + \frac{k_i}{j\omega}. \quad (28)$$

By substituting $G_p(j\omega)$ and $G_c(j\omega)$ in (27b) it is obtained:

$$\bar{k} = \frac{\bar{\omega}_t f_v - \bar{\omega}_t^2 J\tan\left(\bar{m}_\phi - \frac{\pi}{2}\right)}{\bar{\omega}_t J f_v + \tan\left(\bar{m}_\phi - \frac{\pi}{2}\right)} \quad (29)$$

where $\bar{k} = \frac{k_i}{k_p}$. By means of $\bar{k}$ it is possible to compute k_p from (27a):

$$k_p = \frac{\bar{\omega}_t\sqrt{\bar{\omega}_t^2 J^2 + f_v^2}}{\frac{3}{2}p\left(\frac{1}{L_{sy}} - \frac{1}{L_{sx}}\right)\sqrt{\bar{\omega}_t^2 + \bar{k}^2}}. \quad (30)$$

Finally, the value of k_i is obtained as:

$$k_i = \bar{k}k_p. \quad (31)$$

Note that both k_p and k_i are functions of L_{sx} and L_{sy}. This means that there could be a slightly variation with respect to the imposed specification when the design is carried out by means of the nominal values of L_{sx} and L_{sy} but they varies because of the saturation. However, the system will never be unstable (even for very large variation of L_{sx} and L_{sy}) because $G_c(j\omega)G_p(j\omega)$ is a second order system and the phase never crosses -180° (i.e. the gain margin is infinitely large). Alternatively, it is possible to exploit the estimated inductances in order to compute instant by instant the values of k_p and k_i so that the crossover pulsation and the phase margin imposed are always satisfied.

For the *SynRM* drive under test, whose rated data are shown in Tab. I, the following values of crossover pulsation and the phase margin have been imposed:

- $\bar{\omega}_t = 10$ rad/s;
- $\bar{m}_\phi = 55$.

B. Effect of the iron losses

The finite value of the resistance R_0 in the adopted dynamic model is responsible for accounting the iron losses of the SynRM. Such a value has a significant impact on the electromagnetic torque of the *SynRM*. As it is shown in Eq. (9), the electromagnetic torque depends on the vector product between the stator flux and the stator magnetizing space vectors, thus depending on the $\sin(\cdot)$ of the load angle between these two space-vectors. The existence of the iron losses space vector current $\mathbf{i}_0$ causes an increase of the load angle, with respect to the dynamic model of the *SynRM* not accounting for the iron losses ($\mathbf{i}_s = \mathbf{i}_m$). The space-vector representation is shown in Fig. 3. In particular, the classic model not accounting for the iron losses presents a load angle error δ, which is the angle between the stator and magnetizing space vectors. The load angle error δ can be computed as a function of the stator current space vectors and the rotor speed as follows (obtained by applying simple trigonometric rules to the vector diagram in Fig. 3):

$$\delta = \tan^{-1}\left(\frac{|\mathbf{\Psi}_s|\omega_r}{i_{sx}R_0} + \frac{i_{sy}}{i_{sx}}\right) - \tan^{-1}\left(\frac{i_{sy}}{i_{sx}}\right). \qquad (32)$$

The relationship between the load angle error δ in Eq. (32) and the rotor speed and stator current amplitude has been shown for the machine under test in Fig. 4. It clearly highlights that δ increases significantly with the rotor speed, slightly reducing with the stator current, getting values close to 0.7 rad (40°). It implies, as it will clearly shown in the experimental results, that at higher speeds, in particular in field weakening region, a model based controller not accounting for the iron losses can provide stator current space vector references presenting a load angle lower than the real ones, situation that can lead the motor to a close to instability or unstable behavior.

IV. Experimental Set-up

The proposed control technique has been tested experimentally on a suitably developed test set-up with the *SynRM* motor model ABB 3GAL092543-BSB whose rated data are shown in Tab. I. The *SynRM* is mechanically coupled to a torque-controlled Permanent Magnet Synchronous Motor (*PMSM*) drive working as an active load. The *SynRM* is supplied by a Voltage Source Inverter (*VSI*) with Insulated Gate Bipolar Transistor (*IGBT*) modules, model Semikron SMK 50 GB 123, driven by a Space-Vector Pulse Width Modulation (*SV-PWM*) technique with PWM frequency set to 5 kHz. Fig. 5 shows the photo of the *SynRM* drive test set-up. Since it is to be expected that the adaptive input-output *FLC* exhibits its best dynamic performance with respect to rotor oriented control in variable flux working conditions, the control system has been integrated with the *MTPA* proposed in [22].

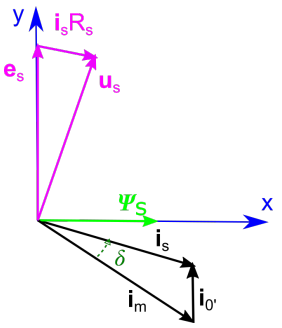

Fig. 3. Space-vector diagram of the *SynRM*.

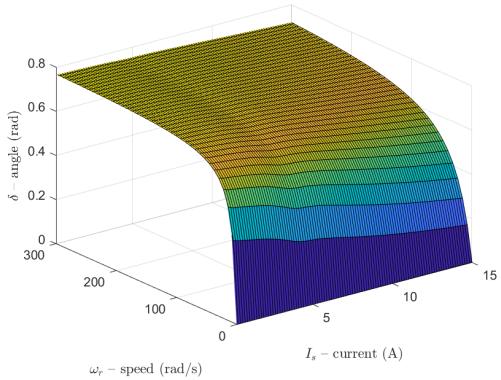

Fig. 4. Load angle error δ surface versus speed and stator current amplitude.

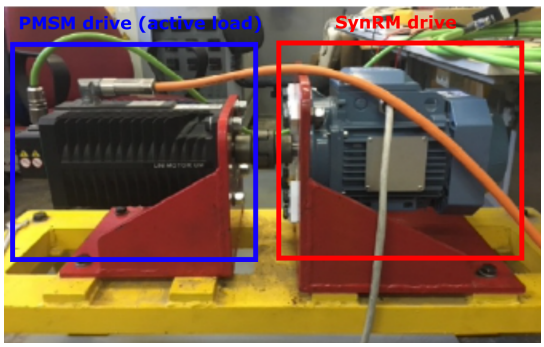

Fig. 5. Photograph of the *SynRM* experimental set-up.

TABLE I
RATED DATA OF THE SYNRM

SYMBOLS	VALUES
Rated power (kW)	2.2
Rated voltage (V)	380
Rated frequency (Hz)	50
Pole-pairs	2
Rated speed (rpm)	1500
Rated current (A)	5.5
Rated torque (Nm)	14
Inertia momentum (kg·m^2)	0.00351

TABLE II
PARAMETERS OF THE *SynRM* MODEL

SYMBOL	VALUE	SYMBOL	VALUE
α_1	1.2139	γ	0.156
β_1	0.4848	μ_1	2.161
η_1	0.0111	σ_1	0.622
α_2	0.3609	μ_2	3.343
β_2	0.4033	σ_2	0.971
η_2	0.0042	R_0	8142

V. EXPERIMENTAL RESULTS

The experimental results have been performed exploiting the test set-up described in section IV. In [15] it has already experimentally shown that the *FLC* outperforms *FOC* in terms of dynamic performance, in both constant flux and variable flux (*MTPA*) working conditions, particularly in variable flux ones. In the following, the proposed input output adaptive *FLC* has been experimentally compared with its corresponding non-adaptive version with fixed inductances. With specific regard to non-adaptive *FLC* with fixed inductances, two values of L_{sx} and L_{sy} have been chosen corresponding to two configurations. Configuration 1) is related to maximum values of L_{sx} and L_{sy} corresponding to the values obtainable theoretically at zero i_{sx}, i_{sy} currents. Configuration 2) is related to 1/2 of the maximum values of L_{sx} and L_{sy}. The constant static inductances corresponding to configuration 1) can be considered correctly tuned in the no-load operation of the *SynRM* drive, while must be considered detuned when the drive is loaded with medium/high load torques. On the contrary, constant static inductances corresponding to configuration 2) can be considered correctly tuned when the drive is loaded with medium/high load torques, while must be considered detuned in the no-load operation.

Since the proposed *FLC* is dedicated to current control, both the adaptive and non-adaptive versions of this *FLC* are expected to theoretically present analogous dynamic performance of the speed loop, in the working conditions in correspondance to which the non-adaptive *FLC* is correctly tuned. In all the tests, the control system has been integrated with the *MTPA* proposed in [22]. Four kinds of experimental tests have been performed and will be described in the following: a. Dynamic response, b. load rejection, c. sensitivity to R_s variation, d. effects of iron losses.

A. Dynamic response

The first test is a speed dynamic test, where a set of speed step references including a speed reversal from 60 to -60 rad/s rad/s has been given to the *SynRM* drive at no load. The test has been performed with the proposed adaptive *FLC* as well as with the non-adaptive one, in both configurations 1 and 2 (in the following simply called non-adaptive *FLC1* and non-adaptive *FLC2*). Fig. 6 shows the reference and measured speeds obtained during this test. It can be observed that the measured speed properly tracks its reference with very high dynamic performance with both the adaptive and non-adaptive *FLCs*, as expected. It can be specifically observed that the adaptive *FLC* and the non-adaptive *FLC1* present good dynamic performance, with negligible differences. There are few conditions in which the non-adaptive *FLC1* slightly outperforms the adaptive *FLC*, which is to be expected since, in these working conditions, the non-adaptive *FLC1* is correctly tuned presenting correct values of L_{sx}, L_{sy}, while the adaptive *FLC* needs to estimate it on-line at the end of each speed transient. As matter of fact, the dynamics of the inductances estimation slightly interfere with the control action, even if with almost negligible effects. On the contrary, the non-adaptive *FLC2* presents worse dynamic performance, as expected since it corresponds to a detuned configuration. It should be further noted an asymmetric behavior in the positive and negative regions. The reason is that, during the positive speed transients, the machine is accelerating, thus the electromagnetic torque must cope not only the inertial torque but also the friction braking torque. As a result, the system is overdamped or slightly underdamped. On the contrary, in the negative speed region, the machine is decelerating, thus the electromagnetic torque must still cope the inertial torque but is helped by the friction braking torque. As a result, the behavior of the controller is more underdamped and presents bigger overshoot. It is not a bad behavior of the proposed controller, while it is due to the conditions of the test.

Fig. 7 shows the corresponding waveforms of the reference and measured i_{sx} and i_{sy} current components. In particular, i_{sy} presents step variations occurring at each speed transient command; i_{sx} presents a similar waveform thanks to application of the *MTPA* in [22]. It can be observed that with the proposed adaptive *FLC* both current components properly track their references, with very high dynamic performance with null tracking error thanks to the on-line estimation of L_{sx}, L_{sy}. As a matter of fact, given the structure of the current controller presenting a *PD* (proportional derivative) structure (without an integral one) - see Eq.s (20) - a null steady state error in current control can be achieved only with the proposed adaptive *FLC*, since the estimated static inductances track the real ones in each operating condition (speed and load). As for the non-adaptive *FLCs*, the configuration 1 permits the stator current properly track their references, since it corresponds to a tuned configuration. Conversely, the configuration 2 corresponds to a detuned condition with evident non-null tracking error.

Fig. 8 shows the corresponding waveform of the estimated direct and quadrature components of the static inductances L_{sx} and L_{sy}. The initial values of the estimated inductances have been purposely set to detuned values, specifically $L_{sx0} = 0.2$ H, $L_{sy0} = 0.2$ H in order to verify that the proposed adaptive *FLC* is able to estimate the correct L_{sx} and L_{sy}, even starting from an initial condition which is not close to the correct one.

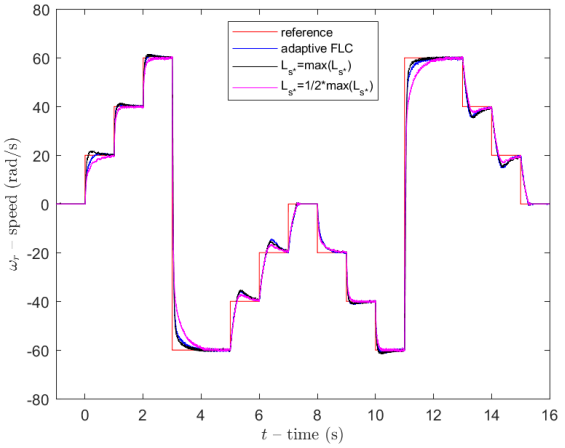

Fig. 6. Reference and measured speed during a dynamic speed test at no-load (experimental).

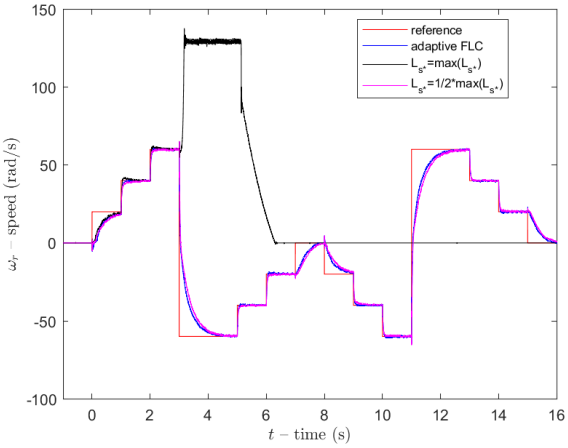

Fig. 9. Reference and measured speed during a dynamic speed test with 5 Nm load torque (experimental).

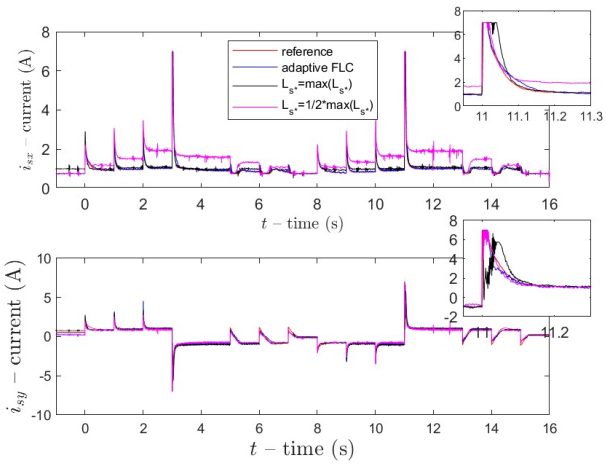

Fig. 7. Reference and measured i_{sx}, i_{sy} during a dynamic speed test at no-load (experimental).

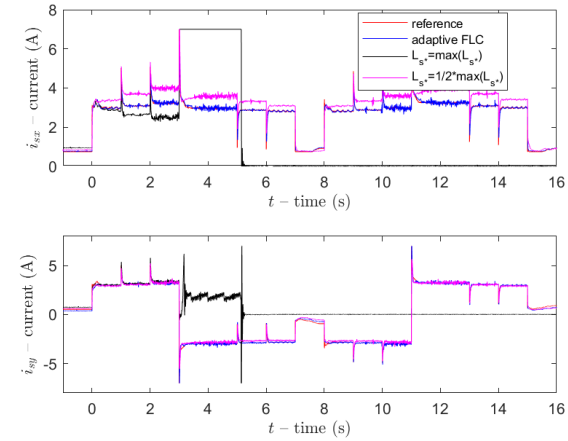

Fig. 10. Reference and measured i_{sx}, i_{sy} during a dynamic speed test with 5 Nm load torque (experimental).

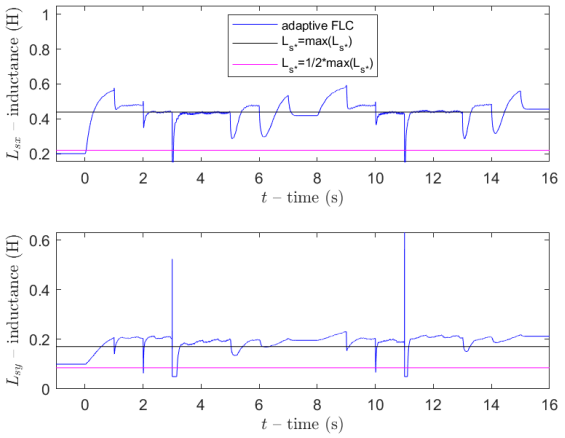

Fig. 8. Reference and measured L_{sx}, L_{sy} during a dynamic speed test at no-load (experimental).

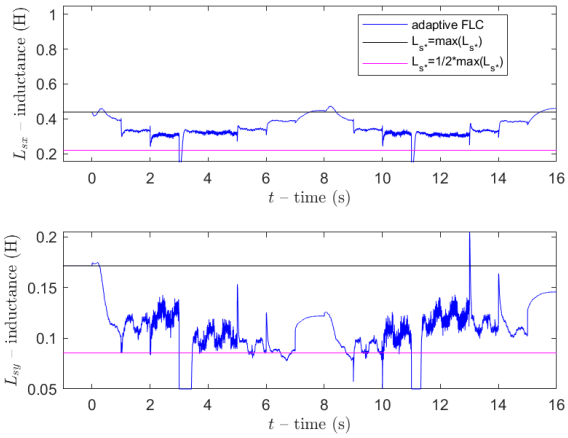

Fig. 11. Reference and measured L_{sx}, L_{sy} during a dynamic speed test with 5 Nm load torque (experimental).

It can be observed that, starting from the initial detuned values of L_{sx} and L_{sy} the on-line estimations of the inductances is activated at each speed transient, as expected from the adaptation law in Eq. (19), showing that the estimation of L_{sx} (L_{sy}) is activate whenever the flux tracking error on the quadrature axis $\psi^*_{sy} - \psi_{sy}$ (direct axis - $\psi^*_{sx} - \psi_{sx}$) axis is nonnull. Moreover, the estimated inductances get their correct values corresponding to each working conditions. As a matter of fact, the test has been made at no load, so for each steady state value of the speed the only present load is the mechanical friction. The higher the speed is, the higher the friction torque is and the higher i_{sx} and i_{sy} are. It justifies why the estimated steady-state values of the inductances slightly vary at each speed transient and, in particular, they decrease a little at higher speeds, particularly L_{sx}. This phenomenon is less observable on the estimated L_{sy}, since the quadrature axis is less sensible to the magnetic saturation. The same test has been performed with a constant load torque of 5 Nm (medium load). In this case, the load torque has been generated properly commanding the *PMSM* torque controlled drive used as active load (see Fig. 5). Fig.s 9, 10 and 11 show respectively the speed, the stator current component and the estimated static inductances waveforms. It is interesting to note that this test case is the dual of the former one. In this case the adaptive *FLC* always permits very good dynamic performance to be achieved. On the contrary, while the non-adaptive *FLC2* correctly behaves with dynamic performance similar to those of the adaptive *FLC*, the the non-adaptive *FLC1* presents an unstable behavior during the speed reversal. It is coherent with the fact that, in presence of medium load, the non-adaptive *FLC2* is correctly tuned, while the non-adaptive *FLC1* is not. Tab. III shows the *IAE* (Integral Absolute Error) computed on the machine speed and stator current components i_{sx}, i_{sy} with the 3 *FLC* techniques in all the experimental tests. It shows results coherent with the above considerations.

B. Load rejection

The second test is a load rejection test, where the *SynRM* drive has been operated at the constant speed of 30 rad/s and a set of increasing load torque steps has been provided to the drive of the type $2 \rightarrow 4 \rightarrow 6 \rightarrow 8$ Nm.

Also in this case, the test has been performed with both the adaptive and non-adaptive versions of the *FLC*. Fig. 12 shows the reference and measured speeds obtained during this test. It can be observed that the measured speed properly tracks its reference with very high dynamic performance, as expected. It can be further observed that the proposed adaptive and non-adaptive versions of the *FLC* do not present significant differences as for the speed dynamics, as expected given that speed control is performed with a classic PI controller tuned with the same parameters in both cases. Fig. 13 shows the corresponding waveforms of the reference and measured i_{sx} and i_{sy} current components. In particular, i_{sy} presents a step increase occurring at each load torque step increase; i_{sx} presents a similar waveform thanks to application of the *MTPA* in [22]. It must be noted that while the proposed adaptive *FLC* permits a null current steady state tracking error in each

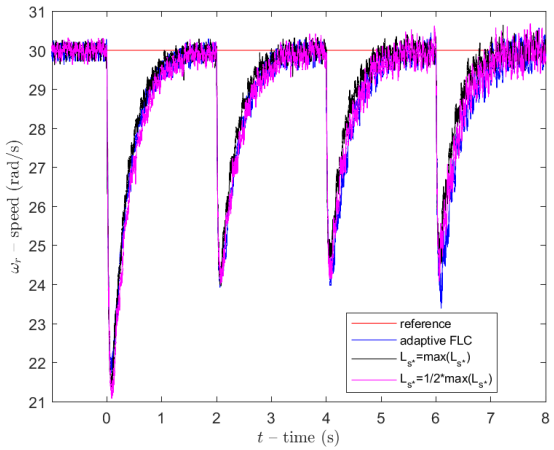

Fig. 12. Reference and measured speed during a load rejection test (experimental).

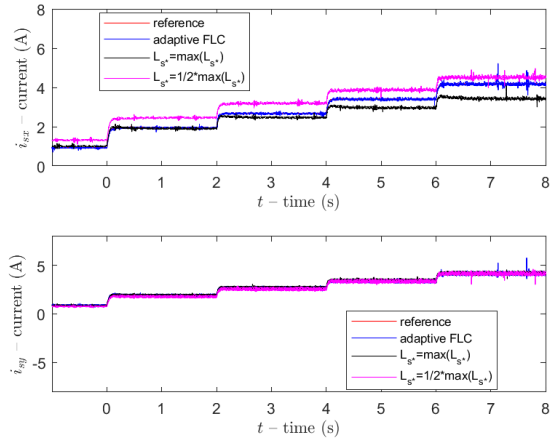

Fig. 13. Reference and measured i_{sx}, i_{sy} during a load rejection test (experimental).

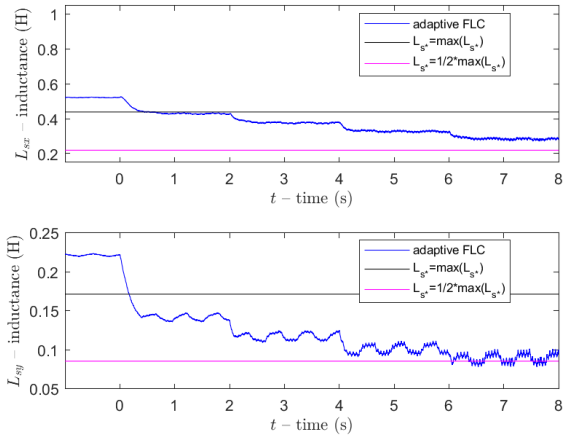

Fig. 14. Reference and measured L_{sx}, L_{sy} during a load rejection test (experimental).

working condition, thanks to the on-line estimation of the inductances, the non-adaptive *FLCs* both present a non-null current tracking error; in particular, the higher the load is, the higher the current tracking error is. Given the notable variations of the static inductances with the working condition, this justifies the adoption of the proposed adaptive *FLC*.

Finally, Fig. 14 shows the corresponding waveform of the estimated direct and quadrature components of the static inductances L_{sx} and L_{sy}. The inductance estimation is activated at each application of the load torque. The higher the load torque is, the higher i_{sx} and i_{sy} are. For this reason a reduction of the estimated inductance is observable for increasing values of the load. This phenomenon more observable on the estimated L_{sx} and less observable on the estimated L_{sy}, since the quadrature axis is less sensible to the magnetic saturation. The speed figure shows basically the same results obtained with both the adaptive and non-adaptive *FLCs*, even with different stator current values. The explanation of such phenomenon is the following. The speed controller outputs a reference quadrature current that is almost equal (small differences) in both the adaptive *FLC* and non-adaptive *FLCs*. However, because of the above considerations, while the adaptive *FLC* permits a null steady-state error, the non-adaptive *FLCs* always present a significant tracking error. Specifically, in the non-adaptive *FLC1* (*FLC2*) i_{sx} is lower (higher) than its reference and lower (higher) than the i_{sx} with the adaptive *FLC*. For lower values of i_{sx} the real L_{sx} of the machine is higher because of the strong saturation on the direct axis. It thus happens that the reduction i_{sx} and the increase of L_{sx} in the non-adaptive *FLC1* somehow compensates each other, leading to similar results obtainable with the adaptive *FLC*. Analogous considerations can be made for the non-adaptive *FLC2*.

C. Sensitivity to R_s variation

The third test is dedicated to the analysis of the sensitivity of the proposed adaptive *FLC* to the variation of the stator resistance R_s. In details, it has been verified experimentally if the proposed controller is able to correctly behave, in a stable way and with sufficient dynamic performance, even if the stator resistance parameter given to the *FLC* is completely detuned. As it is well known, the effect of the detuning of R_s is much more visible at low rotating speeds. For this reason, the adaptive *FLC* has been experimentally tested with a 5 rad/s speed step reference at no load. The test has been performed three times, with R_s^* given to the controller correctly tuned ($R_s^* = R_s$) and strongly detuned ($R_s^* = 10R_s$, $R_s^* = 0.1R_s$). Fig. 15 shows the reference and measured speeds and the reference and measured i_{sx}, i_{sy}. It can be observed that, even with the stator resistance of the controller highly detuned (in an unrealistic way), the *FLC* is still able to work in a stable way, with an acceptable dynamic performance. The *FLC* present a non-null stator current tracking error in both detuned working conditions, as expected. It must be noted that the worst working condition is that with $R_s^* = 0.1R_s$, where the speed response presents a negligible time lag with respect to the reference, even if the higher current tracking error is observable with $R_s^* = 10R_s$. These are, however, unrealistic extreme cases.

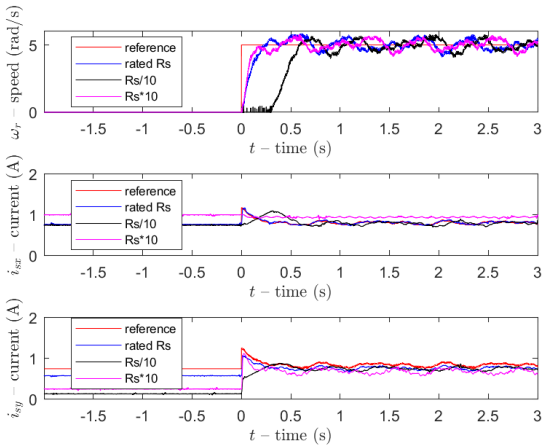

Fig. 15. Speed response to a 5 rad/s speed step reference at no load (experimental).

D. Effects of iron losses

The third test is dedicated to the analysis of the effect of the iron losses resistance R_0 on the performance of the *SynRM* drive. In Section III.A it has been shown that the iron losses resistance R_0 has a significant impact on the electromagnetic torque of the *SynRM*. In particular, neglecting R_0 implies the arise of a load angle error increasing significantly with the rotor speed and slightly reducing with the stator current amplitude. For these reasons, two speed step references at high speeds, respectively 250 and 350 rad/s in the field weakening region, have been given to the drive. At $t = 3$ s, a load step torque has been given to the drive equal to 6 Nm in the 250 rad/s test and equal to 4 Nm in the 350 rad/s test. Fig.s 16 and 17 show the reference and measured speeds as well as the measured current components in the above mentioned tests. The tests have been performed twice, respectively adopting the proposed model accounting for the iron losses (finite value of R_0) and adopting the classic model not accounting for them (infinite value of R_0). Both tests show that the proposed *FLC* accounting for the iron losses correctly behaves even at very high speed in presence of a load torque, presenting a stable behavior and a very limited speed tracking error. On the contrary, if the iron losses are neglected in the model underlying the *FLC*, the 250 rad/s test shows the arise of a big speed tracking error in presence of the load, while the 350 rad/s test shows an unstable behavior of the drive with highly oscillating stator current components and a huge speed tracking error. This behavior is coherent with the analysis in Section III.A and fully justifies the adoption of the proposed model.

VI. Conclusion

In this paper an adaptive input-output *FLC* techniques for *SynRM* drives, taking into consideration the iron losses, has been proposed, where static inductances have been on-line estimated. It has been shown that the on-line estimation of the *SynRM* static inductances allows the magnetic saturation phenomena on both axes to be considered. The stability of

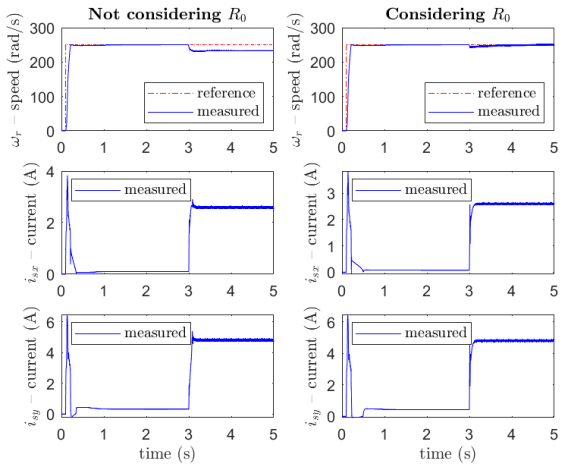

Fig. 16. Reference and measured speed, i_{sx}, i_{sy} during a 250 rad/s speed test with step load application (experiment).

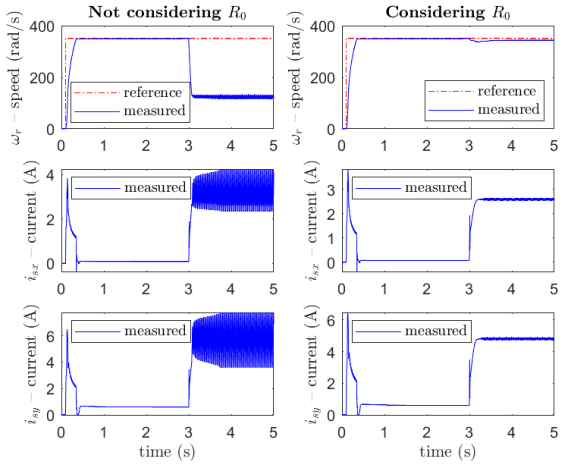

Fig. 17. Reference and measured speed, i_{sx}, i_{sy} during a 350 rad/s speed test with step load application (experiment).

TABLE III
IAE INDEX $J_{IAE} = \int_0^{t_f} |e(t)|dt$

TEST	SPEED $e=\omega^*-\omega$	i_{sx}-CURRENT $e=i^*_{sx}-i_{sx}$	i_{sy}-CURRENT $e=i^*_{sy}-i_{sy}$
A. Dynamic responce (No-load)			
Adaptive FLC	40.43	0.6598	1.602
Non-Adaptive FLC1	39.94	0.908	1.75
Non-Adaptive FLC2	45.81	13.46	2.402
B. Load rejection			
Adaptive FLC	11.07	0.1875	0.5745
Non-Adaptive FLC1	10.41	4.986	0.8731
Non-Adaptive FLC2	10.98	2.471	0.7943
C. Sensitivity to R_s variation			
Rated R_s	1.534	0.113	0.316
$R_s/10$	3.483	0.285	0.461
$10R_s$	1.726	0.781	0.776
D. Effects of iron losses			
250 rad/s with R_0	19.67	0.202	0.891
250 rad/s without R_0	52.71	1.551	3.049
350 rad/s with R_0	38.37	0.886	2.615
350 rad/s without R_0	346.2	5.606	11.55

the control system, as well as the estimation error, has been proved by using a Lyapunov based approach. The proposed control technique has been tested experimentally on a suitably developed test set-up, and the results confirm the effectiveness of the proposed method. Moreover, the comparison of the proposed adaptive *FLC* with its non-adaptive version shows that a null current steady state tracking error can be achieved only thanks to the on line estimation of the static inductances. A sensitivity analysis of the performance of the adaptive *FLC* to the variations of the stator resistance at low speed has shown that the *SynRM* drive is able to correctly behave with good performance even in case of big variations the stator resistance. Finally, the analysis of the effects of the iron losses on the control performance and stability at high speed in the field weakening region at medium/high loads has highlighetd the importance of considering such effects in the adopted model.

REFERENCES

[1] A. Accetta, M. Cirrincione, F. D'Ippolito, M. Pucci, and A. Sferlazza, "Input-output feedback linearization control with on-line inductances estimation of synchronous reluctance motors," in *Energy Conversion Congress and Exposition*. IEEE, 2021, pp. 4973–4978.

[2] P. Vas, *Sensorless vector and direct torque control*. Oxford university press Oxford, UK, 1998.

[3] L. Xu, X. Xu, T. A. Lipo, and D. W. Novotny, "Vector control of a synchronous reluctance motor including saturation and iron loss," *IEEE Transactions on Industry Applications*, vol. 27, no. 5, pp. 977–985, 1991.

[4] R. E. Betz, R. Lagerquist, M. Jovanovic, T. J. Miller, and R. H. Middleton, "Control of synchronous reluctance machines," *IEEE Transactions on Industry Applications*, vol. 29, no. 6, pp. 1110–1122, 1993.

[5] A. Vagati, M. Pastorelli, and G. Franceschini, "High-performance control of synchronous reluctance motors," *IEEE Transactions on Industry Applications*, vol. 33, no. 4, pp. 983–991, 1997.

[6] F.-J. Lin, S.-G. Chen, M.-S. Huang, C.-H. Liang, and C.-H. Liao, "Adaptive complementary sliding mode control for synchronous reluctance motor with direct-axis current control," *IEEE Transactions on Industrial Electronics*, vol. 69, no. 1, pp. 141–150, 2021.

[7] A. Zanelli, J. Kullick, H. M. Eldeeb, G. Frison, C. M. Hackl, and M. Diehl, "Continuous control set nonlinear model predictive control of reluctance synchronous machines," *IEEE Transactions on Control Systems Technology*, vol. 30, no. 1, pp. 130–141, 2021.

[8] H. A. A. Awan, S. E. Saarakkala, and M. Hinkkanen, "Flux-linkage-based current control of saturated synchronous motors," *IEEE Transactions on Industry Applications*, vol. 55, no. 5, pp. 4762–4769, 2019.

[9] H. Hadla and F. Santos, "Performance comparison of field-oriented control, direct torque control, and model-predictive control for SynRMs," *Chinese Journal of Electrical Engineering*, vol. 8, no. 1, pp. 24–37, 2022.

[10] K. A. Maa, B. Arundhati, and M. P. Kumar, "Design, performance of the speed control of a nonlinear variable reluctance motor drive using exact feedback linearization," in *Annual India Conference*, vol. 1. IEEE, 2008, pp. 57–64.

[11] H. A. Zarchi, J. Soltani, A. Maleknia, and G. R. A. Markadeh, "A Lyapunov based nonlinear speed tracking controller for synchronous reluctance motor using adaptive input-output feedback linearization technique," in *International Conference on Industrial Technology*. IEEE, 2008, pp. 1–5.

[12] H. A. Zarchi, J. Soltani, and G. A. Markadeh, "Adaptive input-output feedback-linearization-based torque control of synchronous reluctance motor without mechanical sensor," *IEEE Transactions on Industrial Electronics*, vol. 57, no. 1, pp. 375–384, 2010.

[13] H.-D. Lee, S.-J. Kang, and S.-K. Sul, "Efficiency-optimized direct torque control of synchronous reluctance motor using feedback linearization," *IEEE Transactions on Industrial Electronics*, vol. 46, no. 1, pp. 192–198, 1999.

[14] M. Nabipour, H. A. Zarchi, and S. Madani, "Robust position control of synchronous reluctance motor drives using linear variable structure and adaptive input-output feedback linearization approaches," in *Iranian Conference on Electrical Engineering*. IEEE, 2011, pp. 1–5.

[15] A. Accetta, M. Cirrincione, M. Pucci, and A. Sferlazza, "Feedback linearization based nonlinear control of SynRM drives accounting for self-and cross-saturation," *IEEE Transactions on Industry Applications*, vol. 58, no. 3, pp. 3637–3651, 2022.
[16] ——, "Space-vector state dynamic model of SynRM considering self- and cross-saturation and related parameter identification," *IET Electric Power Applications*, vol. 14, no. 14, pp. 2798–2808, 2020.
[17] ——, "A saturation model of the synchronous reluctance motor and its identification by genetic algorithms," in *Energy Conversion Congress and Exposition*. IEEE, 2018, pp. 4460–4465.
[18] A. Vagati, M. Pastorelli, F. Scapino, and G. Franceschini, "Impact of cross saturation in synchronous reluctance motors of the transverse-laminated type," *IEEE Transactions on Industry Applications*, vol. 36, no. 4, pp. 1039–1046, 2000.
[19] Z. Qu, T. Tuovinen, and M. Hinkkanen, "Inclusion of magnetic saturation in dynamic models of synchronous reluctance motors," in *International Conference on Electrical Machines*. IEEE, 2012, pp. 994–1000.
[20] N. Bedetti, S. Calligaro, and R. Petrella, "Stand-still self-identification of flux characteristics for synchronous reluctance machines using novel saturation approximating function and multiple linear regression," *IEEE Transactions on Industry Applications*, vol. 52, no. 4, pp. 3083–3092, 2016.
[21] A. Accetta, M. Cirrincione, M. Pucci, and A. Sferlazza, "Space-vector state dynamic model of the synchronous reluctance motor considering self, cross-saturation and iron losses," in *Energy Conversion Congress and Exposition*. IEEE, 2021, pp. 4164–4170.
[22] A. Accetta, M. Cirrincione, M. C. Di Piazza, G. La Tona, M. Luna, and M. Pucci, "Analytical formulation of a maximum torque per ampere (MTPA) technique for SynRMs considering the magnetic saturation," *IEEE Transactions on Industry Applications*, vol. 56, no. 4, pp. 3846–3854, 2020.
[23] M. Cirrincione, M. Pucci, G. Cirrincione, and G.-A. Capolino, "A new adaptive integration methodology for estimating flux in induction machine drives," *IEEE Transactions on Power Electronics*, vol. 19, no. 1, pp. 25–34, 2004.

Angelo Accetta (M'08) received his master's degree in Electrical Engineering in 2008, at the University of Palermo, where, in 2011, he obtained the Ph.D. in Electrical Engineering, in collaboration with the Institute for Studies on Intelligent Systems for Automation (ISSIA) - National Research Council (CNR). From 2013 to 2018 he was a Junior Researcher at the Section of Palermo of ISSIA-CNR, Palermo, Italy, working to new energy management strategies for distributed generation systems and to the implementation of new sensorless control strategies for permanent magnets synchronous electric motors (PMSM) and for induction motors both rotating (RIM) and linear (LIM). He is currently Junior Researcher at the INstitute of Marine engineering (INM)-CNR. His research interest are sensorless control systems for electric drives with induction, rotating and linear, motors, with particular attention to their applications for electric generation systems and electric propulsion.

Maurizio Cirrincione (M'03–SM'10) received the Laurea degree in electrical engineering from the Polytechnic University of Turin, Turin, Italy, in 1991 and the Ph.D. degree in electrical engineering from the University of Palermo, Italy, in 1996. From 1996 to 2005, he was a Researcher with the ISSIA-CNR Section of Palermo (Institute on Intelligent Systems for Automation), Palermo, Italy. In September 2005, as a full Professor he join the University of Technology of Belfort-Montbeliard, Belfort, France. He is currently the Head of the "School of Engineering and Physics" of the University of the South Pacific in Suva, Fiji. His current research interests are neural networks for modeling and control, system identification, intelligent control, power electronics, renewable energy systems, and electrical machines and drives. Dr. Cirrincione was awarded the 1997 "E.R.Caianiello" prize for the best Italian Ph.D. thesis on neural networks.

F ilippo D'Ippolito (M'00) was born in Palermo, Italy, in 1966. He received the Laurea degree in Electronic Engineering from the University of Palermo in 1991. He received the Research Doctorate degree in Systems and Control Engineering from the University of Palermo in 1996. He is currently a Research Associate in the Department of Systems and Control Engineering at the University of Palermo. His research interests include control of electrical drives, control of electrical power converters, adaptive and visual/force control of robot manipulators, rehabilitation robotics, marine robotics. Dr. D'Ippolito received the 2000 Kelvin Premium from the Institution of Electrical Engineers (IEE), for the paper "Parameter identification of induction motor model using genetic algorithms".

Marcello Pucci (M'03–SM'11) received the Laurea and Ph.D. degrees in electrical engineering from the University of Palermo, Italy, in 1997 and 2002, respectively. In 2000, he was a Host Student with the Institute of Automatic Control, Technical University of Braunschweig, Braunschweig, Germany, working in the field of control of ac machines, with a grant from the German Academic Exchange Service. From 2001 to 2018, he has been with the Institute of Intelligent Systems for Automation, Section of Palermo, National Research Council of Italy. Currently he is a Senior Researcher at the INstitute of Marine engineering (INM)-CNR. His current research interests include electrical machines; control, diagnosis, and identification techniques of electrical drives; and intelligent control and power converters. Dr. Pucci serves as an Associate Editor for the IEEE transactions on industrial electronics and IEEE transactions on industry applications. He is a member of the Editorial Board of the Journal of Electrical Systems.

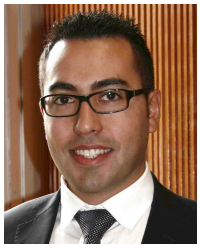

Antonino Sferlazza (S'12–M'15) was born in Palermo, Italy, in 1987. He received the Master degree in automation engineering and the Ph.D. degree in mathematics and automation from the University of Palermo, Italy, in 2011 and 2015 respectively. In 2013 he was visiting PhD student at University of California at Santa Barbara, CA, USA, in the field of modeling and analysis of stochastic hybrid systems. From 2016 to 2017 he join the University of Palermo as junior researcher. From 2017 to 2018 he was researcher are LAAS CNRS of Toulouse, France, working in the field of control of power converter. He is currently a researcher in systems and control engineering at the University of Palermo. His research interests include the development of feedback control algorithms for nonlinear dynamical systems, optimization techniques, estimation of stochastic dynamical systems, and applications of control of electrical drives, power converters, and mechanical systems.